Hindawi Publishing Corporation
Advances in OptoElectronics
Volume 2007, Article ID 27316, 7 pages
doi:10.1155/2007/27316

Research Article

nm- and μm-Scale Surface Roughness on Glass with Specific Optical Scattering Characteristics on Demand

Henning Fouckhardt,[1] Ingo Steingoetter,[1] Matthias Brinkmann,[2] Malte Hagemann,[2] Helmut Zarschizky,[3] and Lin Zschiedrich[3]

[1] *Integrated Optoelectronics and Microoptics Research Group, Physics Department, Kaiserslautern University of Technology, P.O. Box 3049, D-67653 Kaiserslautern, Germany*
[2] *Faculty of Mathematics and Science, Darmstadt University of Applied Sciences, Haardtring 100, D-64295 Darmstadt, Germany*
[3] *JCMwave GmbH, Haarer Straße 14a, D-85640 Putzbrunn, Germany*

Received 10 January 2007; Accepted 20 April 2007

Recommended by Stefan A. Maier

During maskless ion etching of amorphous glass, self-organization can arise in certain etch parameter ranges, which leads to dense-lying dots/cones with typical diameters and heights in the 30–300 nm range. Another phenomenon, which results in cone sizes around 1 μm or more, is self-masking especially in the case of heterogeneous glasses like borosilicate glass as used in this contribution. Thus, a wide range of characteristic sizes and shapes of individual scatterers on the glass surface, jointly acting as a defined roughness, can be achieved resulting in specific optical scattering characteristics. This contribution gives results on borosilicate thin-glass dry etching. Certain surface morphologies are reported together with experimental results on their optical scattering characteristics.

1. INTRODUCTION

Optics and laser physics are enabling technologies for the 21st century. Light sources and optical elements have to be tailored very specifically depending on application. Glasses have become important materials for functional substrates of devices and modules. Transmission, reflection, scattering loss, and spatial scattering distribution or an inherent antireflection function of the front facet a la moth's eye effect [1] have to be controlled and tailored. Thus, more and more optical substrates do not just have to provide for mechanical stability of the devices, but should incorporate optical functions—including certain scattering characteristics. For example, in organic light emitting diode (OLED) technology, care has to be taken such that as much of the electroluminescence as possible is not guided sideways out of the OLED by total internal reflection, but rather leaves the device perpendicularly to the emitting layer sequence (see, e.g., [2, 3]). Or substrates for thin film solar cells could redirect the light power portion, not absorbed during the first passage through the active layers, back into that layer sequence to give higher efficiency. The possible applications for certain scattering characteristics are manifold.

One approach to achieve rough optical surfaces on purpose is pulsed-laser ablation and even pulsed-laser assisted growth [4–6]. On the other hand, as scanning techniques, these approaches cannot easily be upscaled to large substrates. A maskless nonscanning procedure is favorable.

Far back between 1956 and 1962, Navez et al. [7] ion-beam-bombarded glass surfaces and observed some unexpected surface morphologies: wave-like structures for flat ion beam incidence and dots/cones for nearly perpendicular incidence. Typical wave periods and characteristic dot sizes were in the range of some 10 nm to some 100 nm. As described in a review article by Valbusa et al. [8], subsequently, many groups picked up these investigations—not only with (reactive) ion-beam machines, but also with (reactive) ion etching (RIE). Those investigations were usually not performed with amorphous glass, but rather for semiconductors or even metals [9–23]. The phenomenon observed and described in all of these publications is *self-organization* due to two compensating effects, which together stabilize the surface profile: first a tendency of surface structure shrinkage due to a preferred etch erosion at oblique flanks and secondly diffusion of the eroded particles into the etched depressions

and adsorption. Theoretical description is based on the so-called damped Kuramoto-Sivashinsky equation for the rate of the height profile change [19, 24–26]. The etch-based dots lie close to each other in the surface plane. Dot shapes (cones, pyramids, ...) depend on dry-etch parameters, like ion energy or ion-beam divergence.

Another important phenomenon at least in glass etching is self-masking [27]. Especially for heterogeneous glasses like the inexpensive borosilicate glass, certain components can give new nonvolatile compounds during wet or dry etching, which function as a randomly distributed ensemble of usually undesired tiny etch masks and locally prohibit further etching. These effects give a roughness on the scale of 1 μm to many microns. In an early paper by Affatigato et al. [28], the influence of an initial surface roughness on wet etch rates was investigated, while using optical scattering behavior to characterize the roughness. In our current contribution, however, the scattering characteristics themselves and their dependence on the shape of the single scatterers are in the focus of the interest.

Light scattering at rough microstructured or nanostructured surfaces or by volume scattering centers arranged three-dimensionally within a transparent host material (glass, plastic, etc.) is a classical topic in optics [29–35], but still a field of very active current research. Moreover, modern nano-structuring technologies led to a renaissance of this topic and surface roughness can be employed for new optical functions.

A problem is the lack of sufficiently realistic physical models predicting the scattered light distribution from a given specific surface profile or scattering center arrangement. Moreover, there are only very few attempts to tackle the corresponding inverse problem, that is, designing the surface structure from a desired angular light distribution. Thus thorough investigations have to be performed.

2. HARVEY MODEL

The Harvey model [29, 30] has been developed to describe the optical scattering characteristics, for example, of polished glass surfaces in terms of macroscopic quantities, that is, the specular transmission, diffuse transmission, specular reflection, and diffuse reflection.

In the model, the scattering spot on the surface, on one hand, is regarded as an illuminated surface, which experiences an irradiance E due to the laser light source. On the other hand, this very scattering spot can be seen as a secondary light source, from which a radiation density (radiance) L originates. Thus, the scattering angle (θ, ϕ)- and specular angle (θ_0, ϕ_0)-dependent function *BSDF* (bidirectional scattering distribution function; dimension 1 sr^{-1}; θ is the polar angle while ϕ is the azimuth) emerges [29, 30, 35], which is to be distinguished between the reflection *(BRDF)* and the transmission *(BTDF)* case; see also Figure 1:

$$\mathrm{BSDF} = \frac{L}{E} = \frac{P_{\mathrm{det}}}{A_{\mathrm{spot}} A_{\mathrm{det}} \cos\theta / r^2} \Big/ \frac{P_{\mathrm{laser}}}{A_{\mathrm{spot}}} \tag{1}$$

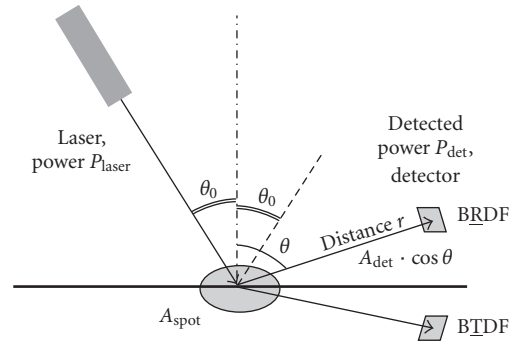

Figure 1: 1-dimensional sketch of scattering situation for definition of certain quantities according to [35].

with the areas A_{spot} and A_{det} of the scattering spot and of the detector, respectively, P_{laser} as laser light power and P_{det} as the light power caught by the detector, r as the distance between the areas A_{spot} and A_{det}. With both *BSDF* functions, that is, *BRDF* and *BTDF*, there are two more functions, that is, the so-called *TIS* for total integrated scattering—again distinguished between reflection (TIS_R) and transmission (TIS_T)—which stand for the ratio of the total scattered light power and the input light power (in the backward or forward direction, respectively), here, exemplarily written for reflection:

$$\mathrm{TIS}_{\underline{R}} = \int_0^{2\pi} \int_0^{\pi/2} \mathrm{B\underline{R}DF}\,(\theta, \phi; \theta_0, \phi_0) \cos\theta \sin\theta d\theta d\phi. \tag{2}$$

With R, T, P_{abs}, and P_{all} as reflected, transmitted, absorbed, and total overall power, respectively, the following equations result with R_d, R_s, T_d, T_s as powers in diffuse reflection, specular reflection, diffuse transmission, and specular transmission:

$$R + T + P_{\mathrm{abs}} = P_{\mathrm{all}}, \tag{3a}$$

$$P_{\mathrm{abs}} = 0 \quad \text{(assumed)}, \tag{3b}$$

$$R_d = \mathrm{TIS}_R \cdot R, \tag{3c}$$

$$R_s = (1 - \mathrm{TIS}_R) \cdot R, \tag{3d}$$

$$T_d = \mathrm{TIS}_T \cdot T, \tag{3e}$$

$$T_s = (1 - \mathrm{TIS}_T) \cdot T. \tag{3f}$$

In our case, T and R are corrected/normalized such that the usual Fresnel reflections at both plane and smooth surfaces of a glass substrate under normal incidence vanish ($R = 0$, $T = 1$).

In most optical scattering experiments, the double-logarithmic dependence of *BSDF* on $\sin\theta$ with θ as polar angle is very similar, the typical trace is shown as a dashed line qualitatively in Figure 2. The trace can be characterized with certain parameters, for reflection or transmission: s as slope of the straight line acting as an asymptotic line for large angles, b_0 as value of the saturation for small scattering angles (second asymptotic line), l as $\sin\theta$ value for the bending point of the trace, that is, the intersection of both asymptotic lines, and sometimes also b as *BSDF* value for a distinct $\sin\theta$ value, for example, for 0.01.

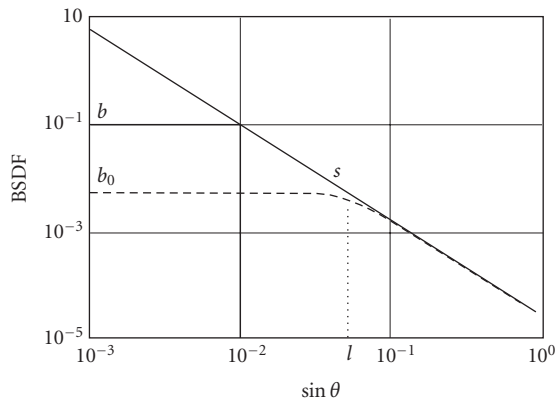

FIGURE 2: Typical qualitative log(BSDF) curve in dependence on log(sin θ) for most scattering surfaces, described with the quantities of the Harvey model according to [35].

3. DRY-ETCHING RESULTS

For most applications, it is favorable to achieve very smooth surfaces during wet or dry glass etching (see, e.g., [27, 36–39] for fused silica). But a paradigm change is taking place, since rough optical surfaces can act as quasilayers with new optical functions.

This contribution focuses on dry etching of borosilicate glass. For certain parameter sets, rough surfaces come up—with dense cone structures and characteristic feature sizes in the range 30–1000 nm, indicating a mixture of both the self-organization as well as the self-masking effect. Dry-etching series with varying process parameters (etch gas composition, etch gas pressure, microwave power in the ion etching machine, substrate holder cooling, etc.) were carried through with D263T borosilicate thin-glass by Schott [40] with a thickness of 110 μm. A RIE plasma etching machine of type MicroSys by Roth & Rau, Wuestenbrand, Germany, with electron cyclotron resonance (ECR) plasma generation was available.

Figure 3 shows scanning electron microscopy (SEM) images and angular scattering power distributions in transmission (colored insets) of several dry-etched borosilicate glass surfaces for some of the applied RIE-etch parameter sets using CF_4/Ar plasmas. These samples were measured and evaluated according to the Harvey model [29, 30, 35] with respect to the following quantities: specular reflection, diffuse reflection, specular transmission, diffuse transmission, and others for monochromatic surface-normal collimated laser beam illumination with a spot diameter of several millimeters onto the smooth surface at 633 nm vacuum wavelength (or 635 nm in other cases).

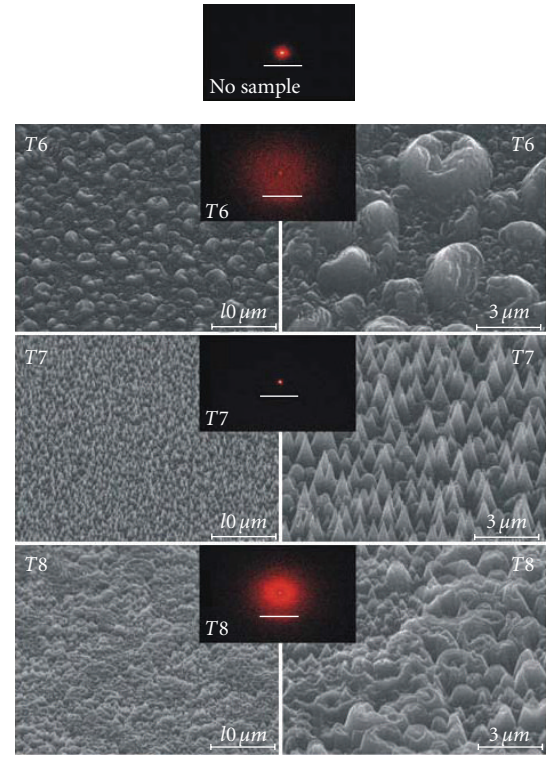

FIGURE 3: SEM images showing dry-etching results. The diversity of the results is a consequence of different dry-etching parameters. The insets give the angular transmitted power distribution for normal incidence onto the smooth surface of the etched glass samples (He−Ne laser beam, vacuum wavelength $\lambda = 633$ nm); the white bars mean $\pm 5^\circ$ far field angle range.

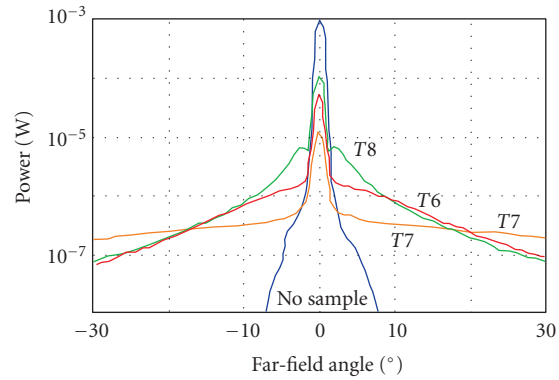

FIGURE 4: Experimental results for the lateral far-field scattering power distribution in transmission from samples T6–T8, illuminated by a collimated laser diode beam (vacuum wavelength $\lambda = 635$ nm).

4. OPTICAL SCATTERING EXPERIMENTS

The overall surface roughness was characterized by light scattering experiments in transmission and in reflection: total transmitted and reflected optical power (using an optical integrating sphere), angular transmission and reflection scattering distribution functions (with a goniometer), and broadening of the specular peaks (far-field set-up).

Figure 4 gives experimental results of the goniometric characterization. For all samples, a collimated laser light beam at 635 nm vacuum wavelength has been launched into the sample substrates from the nonstructured, smooth

surface side. The far-field measurements reveal that there is very little broadening of the specular peak, which makes the diffusely transmitted portion of the light power (T_d) easily evaluated.

Table 1 summarizes results of the scattering experiments in terms of the Harvey model parameters. All samples show the typical $\log(BSDF) = f(\log(\sin\theta))$ traces as predicted by Figure 2, except for sample T8, which reveals an additional small dip in the *BTDF* curve, corresponding to a darker ring around the central specular peak (compare with the 4th inset of Figure 3). For a glass plate with two smooth surfaces (front and back), the loss due to Fresnel reflections is about 8% for surface-normal incidence. But the T and R values of Table 1 are corrected/normalized such that the usual Fresnel reflections vanish ($R = 0$, $T = 1$).

All measurement and evaluation results can be explained by a mixture of diffraction at structures with sizes close to the wavelength and scattering at even smaller features. Sample T6 shows the lowest percentage in total transmitted power (84% instead of 100% (normalized)) and the highest diffuse portion of light power in transmission (99% of the transmitted 84%). This last result is attributed to scattering at the multiterrace-like features on the larger single scatterers.

Sample T7 has the largest transmitted power portion of all samples (89%). The sharp cones of sample T7 seem to act as individual tapers redirecting the light into the forward direction. Of course, the transmission is only 89% instead of 100% (normalized) for a glass slide with two smooth sides. But due to the roughness of one surface of sample T7, undesired waveguiding sideways are strongly reduced and (quasi) specular transmission is high (4.4%). These features should make sample T7 useful as outcoupling enhancing substrate for OLED applications. This has been demonstrated in a first experiment: sample T7 has been stuck on top of a yellow-emitting OLED using a standard index matching oil (cedar wood oil) (see inset of Figure 5 for a sketch of the exact layer sequence, which includes a reflecting Al layer at the bottom side, that is, next to the OLED emitter layers; the inset omits the transparent contact layers). The angle-dependent light outcoupling efficiency, that is, the ratio of the radiance with and without T7 (all other features the same, including the Al reflecting layer) is shown in Figure 5. It is possible to increase the radiance by 20%. Further improvement should be possible, of course, by using a T7-like etched glass sample as the only substrate and growth of the OLED layers onto the smooth (or even onto the other, i.e., rough) side.

Sample T8 shows single scatterers with vulcano-like surface structures with central dome. They can be viewed as diffracting phase objects. The Fourier transform of such objects looks itself similar to these objects; thus, the measured darker ring around the central maximum in the scattering distribution in transmission can be explained.

5. NUMERICAL CALCULATIONS

Due to the fact that its scattering characteristics are especially interesting for applications, the behavior of sample T7 is exemplarily modeled in some detail numerically.

Table 1: Experimentally determined Harvey model parameters of etched borosilicate thin-glass samples T6–T8; the subscript $_T$ stands for quantities b_0, s, ℓ in transmission, $_R$ in reflection. The T and R values of Table 1 are corrected/normalized such that the usual Fresnel reflections at a glass plate with two plane and smooth surfaces under normal incidence vanish ($R = 0$, $T = 1$).

Sample	$T/(T+R)$	T_S/T	T_d/T	$R/(T+R)$
T6	**0.839**	*0.0082*	*0.990*	**0.161**
T7	**0.891**	*0.0440*	*0.951*	**0.109**
T8	**0.852**	*0.0995*	*0.883*	**0.148**

Sample	$T/(T+R)$	$b_{0,T}$	S_T	ℓ_T
T6	**0.839**	0.42	−3.56	0.25
T7	**0.891**	0.72	−2.20	0.50
T8	**0.852**	29.50	−1.86	0.03

Sample	$R/(T+R)$	$b_{0,T}$	S_R	ℓ_R
T6	**0.161**	596	−0.55	10^5
T7	**0.109**	12740	−0.91	10^5
T8	**0.148**	2371	−1.00	10^4

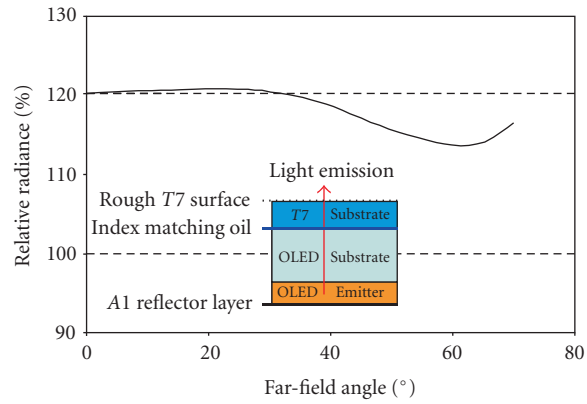

Figure 5: Outcoupling efficiency enhancement for an OLED in case of the use of glass sample T7 as an additional substrate coupled to the OLED by an index matching oil.

Scattering characteristics in transmission and reflection of the samples with rough surfaces can be attributed to diffraction at larger single scatterers and at arrangements of many scatterers as well as scattering at even finer features. Additionally, the interference of the diffracted and/or scattered light has to be considered. To account for all these effects in numerical calculations is nearly impossible even today, especially for non-well-shaped single scatterers and large scattering areas. Thus, we modeled only one, but very important aspect of the situation, that is, the shape of a single scatterer, that is, for sample T7, a cone. The calculation of the single scatterer's shape influence can explain how the scatterer contributes to the rerouting of portions of the light power between transmission and reflection as well as between specular and diffuse portions.

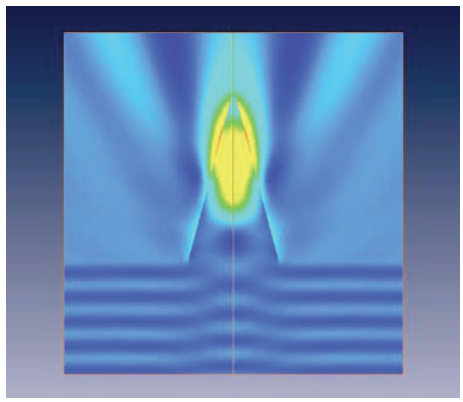

Figure 6: Result of a numerical calculation using the JCMwave software JCMharmony.2D on the diffraction/scattering behavior of a single cone-shaped scatterer of sample T7 with a cone full width at half maximum of 0.8 μm and a height of 1.5 μm. Surface-normal incidence of monochromatic light at 633 nm wavelength leaving the glass substrate (bottom) into air (top in figure) is assumed. The absolute value of the electric field amplitude of the electromagnetic wave is given and coded both as colors and brightness (bright yellow = high value; dark blue = low value).

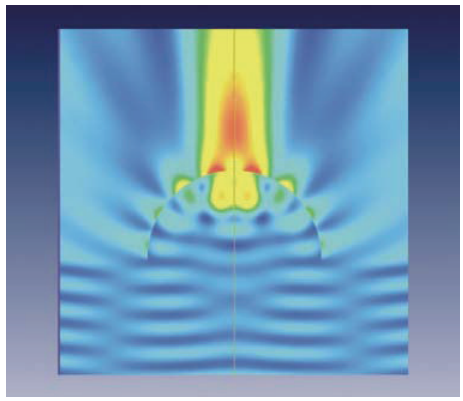

Figure 7: Result of a numerical calculation similar to the one from Figure 6, but now for a hemispherical single scatterer of the same volume as that of the cone from Figure 6. The color coding scale is different for this figure as compared to Figure 6.

We used the software JCMharmony. 2D with a cylinder-symmetrical extension by JCMwave GmbH, Putzbrunn, Germany. It relies on the rigorous solution of Maxwell's equations, using a finite element method (FEM). Especially by employing nonstructured, adaptive finite element meshes, and FEM elements of high orders, these programs show clear advantages in convergence, precision, and calculation speed, when compared to other software solutions [41–44]. In case of cylinder-symmetrical formulations, the use of an appropriate extension of a 2D solver in fact gives full 3D output, but strong reduction of numerical effort.

For sample T7, Figure 6 shows the influence of a single scatterer. The absolute value of the steady state electric field amplitude of the electromagnetic wave is coded both as colors and brightness (bright yellow = high value; dark blue = low value). A monochromatic plane wave at 633 nm wavelength with surface-normal incidence onto the smooth side and from the bottom is assumed for the calculations, corresponding to the experimental situation in connection with the insets of Figure 3. The cone has a geometrical full width at half maximum of 0.8 μm and is 1.5 μm tall. The numerical result reveals how the field amplitude is concentrated in the cone's tip, from where radiation occurs. The calculation has been stationary based on the time harmonic solution of Maxwell's equations.

Thus, the cone structure strongly influences the scattering behavior of sample T7. Each cone can be regarded as a rotationally symmetrical taper, redirecting the light forward. Of course—as illustrated by Figure 3—in reality there is a variety of cone heights, angles, and separations. This distribution or inhomogeneity of cone parameters itself acts as a statistical roughness, increasing the diffuse transmission in comparison to the specular transmission. Future simulations incorporating a couple of scatterers with different parameters have to be performed to investigate this aspect further.

To compare the influence of the cones to other simple scatterers' shapes, we recalculated the situation for a hemispherical single scatterer of the same volume as in the case of the cone in Figure 6, that is, hemisphere radius = 1/2 height of cone. (To some extent this situation comes close to sample T6.) The corresponding numerical result is given in Figure 7.

Again, the scatterer concentrates the field at its very top, from where radiation occurs. As the data in Table 1, for the comparison of samples T6–T8, indicate, this field concentration is the strongest for the cone-shaped scatterer acting as a taper. So the overall transmission is the strongest for sample T7 (89%) and the relative specular transmission (4.4%) is much stronger for sample T7 than for T6 (0.8%).

The situation with hemispherical scatterers partially also resembles efforts to improve OLED outcoupling efficiency by micro lens arrays on top of the OLED structure at the outcoupling side (see, e.g., [45]). But those micro lenses rather have typical sizes in the many microns or even millimeter range.

6. CONCLUSIONS AND OUTLOOK

A self-organization phenomenon and a self-masking effect occurring during maskless dry etching of borosilicate thin glass (and probably many other glasses) can result in rough surfaces with defined roughness over a wide size range from several 10 nm to several microns. Depending on the shape of the single scatterers (and other features), samples show specific optical scattering characteristics, which might be used for certain applications like improvement of OLED or thin-film solar cell efficiency. Further investigations have to be performed to extend shape variety and thus scattering features.

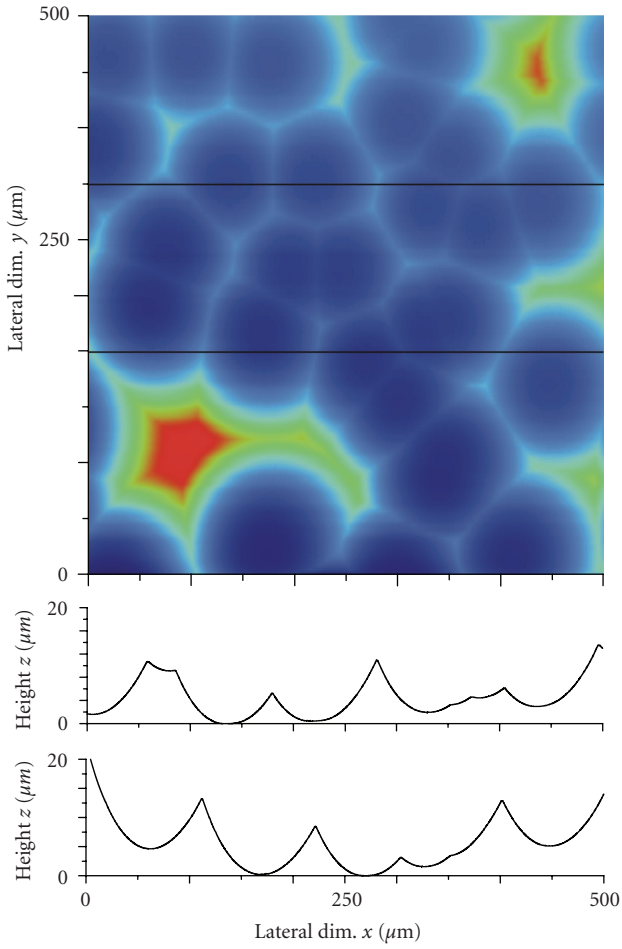

Figure 8: Wet-etch result of a fused silica sample using a hard mask with statistically arranged via holes. The image is a false-color image of a surface profiler. Moreover, two line scans are given.

The roughness range can even be extended by starting with a substrate, which has been prestructured by a wet-chemical etch through a hard etch-mask with statistically arranged via holes, as can be seen in Figure 8, in this case with a fused silica sample (similar to early results by Affatigato et al. [28]) achieved without an etch-mask starting with a roughened surface. The image is a false-color image of a surface profiler. Moreover, two line scans are given (see related lines in colored image), which indicate the color coding and which reveal that the isotropic etch shape is not smoothed out during the etch. In the future this prestructuring of the substrate has to be incorporated into the investigations.

ACKNOWLEDGMENTS

The authors thank Schott AG, Mainz, Germany for the supply of D263T thin-glass sheets and Merck KgaA, Darmstadt, Germany for the supply of OLED samples.

REFERENCES

[1] A. Gombert, W. Glaubitt, K. Rose, et al., "Antireflective transparent covers for solar devices," *Solar Energy*, vol. 68, no. 4, pp. 357–360, 2000.

[2] C. F. Madigan, M.-H. Lu, and J. C. Sturm, "Improvement of output coupling efficiency of organic light-emitting diodes by backside substrate modification," *Applied Physics Letters*, vol. 76, no. 13, pp. 1650–1652, 2000.

[3] M.-H. Lu and J. C. Sturm, "Optimization of external coupling and light emission in organic light-emitting devices: modeling and experiment," *Journal of Applied Physics*, vol. 91, no. 2, pp. 595–604, 2002.

[4] D. H. Lowndes, J. D. Fowlkes, and A. J. Pedraza, "Early stages of pulsed-laser growth of silicon microcolumns and microcones in air and SF_6," *Applied Surface Science*, vol. 154-155, pp. 647–658, 2000.

[5] A. Ben-Yakar, R. L. Byer, A. Harkin, et al., "Morphology of femtosecond-laser-ablated borosilicate glass surfaces," *Applied Physics Letters*, vol. 83, no. 15, pp. 3030–3032, 2003.

[6] R. R. Gattass, L. R. Cerami, and E. Mazur, "Micromachining of bulk glass with bursts of femtosecond laser pulses at variable repetition rates," *Optics Express*, vol. 14, no. 12, pp. 5279–5284, 2006.

[7] M. Navez, C. Sella, and D. Chaperot, "Microscopie electronique—étude de lattaque du verrepar bombardement ionique," *Comptes Rendus de l'Académie des Sciences*, vol. 254, no. 2, p. 240, 1962.

[8] U. Valbusa, C. Boragno, and F. Buatier de Mongeot, "Nanostructuring surfaces by ion sputtering," *Journal of Physics Condensed Matter*, vol. 14, no. 35, pp. 8153–8175, 2002.

[9] G. Carter and V. Vishnyakov, "Roughening and ripple instabilities on ion-bombarded Si," *Physical Review B*, vol. 54, no. 24, pp. 17647–17653, 1996.

[10] F. Frost, A. Schindler, and F. Bigl, "Roughness evolution of ion sputtered rotating InP surfaces: pattern formation and scaling laws," *Physical Review Letters*, vol. 85, no. 19, pp. 4116–4119, 2000.

[11] D. Flamm, F. Frost, and D. Hirsch, "Evolution of surface topography of fused silica by ion beam sputtering," *Applied Surface Science*, vol. 179, no. 1–4, pp. 95–101, 2001.

[12] F. Frost and B. Rauschenbach, "Nanostructuring of solid surfaces by ion-beam erosion," *Applied Physics A*, vol. 77, no. 1, pp. 1–9, 2003.

[13] F. Frost, B. Ziberi, T. Höche, and B. Rauschenbach, "The shape and ordering of self-organized nanostructures by ion sputtering," *Nuclear Instruments and Methods in Physics Research, Section B*, vol. 216, no. 1–4, pp. 9–19, 2004.

[14] S. Facsko, T. Dekorsy, C. Koerdt, et al., "Formation of ordered nanoscale semiconductor dots by ion sputtering," *Science*, vol. 285, no. 5433, pp. 1551–1553, 1999.

[15] S. Facsko, T. Bobek, T. Dekorsy, and H. Kurz, "Ordered quantum dot formation by ion sputtering," *Physica Status Solidi (B)*, vol. 224, no. 2, pp. 537–540, 2001.

[16] S. Facsko, H. Kurz, and T. Dekorsy, "Energy dependence of quantum dot formation by ion sputtering," *Physical Review B*, vol. 63, no. 16, Article ID 165329, 5 pages, 2001.

[17] S. Facsko, T. Bobek, H. Kurz, T. Dekorsy, S. Kyrsta, and R. Cremer, "Ion-induced formation of regular nanostructures on amorphous GaSb surfaces," *Applied Physics Letters*, vol. 80, no. 1, pp. 130–132, 2002.

[18] T. Bobek, S. Facsko, H. Kurz, T. Dekorsy, M. Xu, and C. Teichert, "Temporal evolution of dot patterns during

ion sputtering," *Physical Review B*, vol. 68, no. 8, Article ID 085324, 6 pages, 2003.

[19] S. Facsko, T. Bobek, A. Stahl, H. Kurz, and T. Dekorsy, "Dissipative continuum model for self-organized pattern formation during ion-beam erosion," *Physical Review B*, vol. 69, no. 15, Article ID 153412, 4 pages, 2004.

[20] K. H. Heinig, T. Müller, B. Schmidt, M. Strobel, and W. Möller, "Interfaces under ion irradiation: growth and taming of nanostructures," *Applied Physics A*, vol. 77, no. 1, pp. 17–25, 2003.

[21] P. Sigmund, "A mechanism of surface micro-roughening by ion bombardment," *Journal of Materials Science*, vol. 8, no. 11, pp. 1545–1553, 1973.

[22] S. G. Mayr and R. S. Averback, "Evolution of morphology in nanocrystalline thin films during ion irradiation," *Physical Review B*, vol. 68, no. 7, Article ID 075419, 9 pages, 2003.

[23] M. Posselt, M. Mäder, R. Grötzschel, and M. Behar, "Competing influence of damage buildup and lattice vibrations on ion range profiles in Si," *Applied Physics Letters*, vol. 83, no. 3, pp. 545–547, 2003.

[24] M. Paniconi and K. R. Elder, "Stationary, dynamical, and chaotic states of the two-dimensional damped Kuramoto-Sivashinsky equation," *Physical Review E*, vol. 56, no. 3, pp. 2713–2721, 1997.

[25] R. M. Bradley and J. M. E. Harper, "Theory of ripple topography induced by ion bombardment," *Journal of Vacuum Science & Technology A: Vacuum, Surfaces, and Films*, vol. 6, no. 4, pp. 2390–2395, 1988.

[26] R. H. W. Hoppe, W. G. Litvinov, and S. J. Linz, "On solutions of certain classes of evolution equations for surface morphologies," *Nonlinear Phenomena in Complex Systems*, vol. 6, no. 1, pp. 582–591, 2003.

[27] I. Steingoetter, *Quarzglas-Chips fuer die Kapillarelektrophorese mit leckwellenleitergestuetzter Detektion*, dissertation.de, Berlin, Germany, 2006, Dissertation Fachbereich Physik TU Kaiserslautern.

[28] M. Affatigato, D. H. Osborne, and R. F. Haglund Jr., "Effect of surface roughness on the acid etching of amorphous silica," *Journal of the American Ceramic Society*, vol. 79, no. 3, pp. 688–694, 1996.

[29] C. L. Vernold and J. E. Harvey, "Modified Beckmann-Kirchoff scattering theory for nonparaxial angles," in *Scattering and Surface Roughness II*, vol. 3426 of *Proceedings of SPIE*, pp. 51–56, San Diego, Calif, USA, July 1998.

[30] M. Brinkmann, J. Hayden, M. Letz, et al., "Optical materials and their properties," in *Springer Handbook of Lasers and Optics*, F. Traeger Ed., New York, NY, USA, 2007.

[31] J. M. Elson, H. E. Bennett, and J. M. Bennett, "Scattering from optical surfaces," in *Applied Optics and Optical Engineering*, R. R. Shannon and J. C. Wyant, Eds., vol. 7, chapter 7, p. 191, Academic, New York, NY, USA, 1979.

[32] H. C. van de Hulst, *Light Scattering by Small Particles*, Dover, New York, NY, USA, 1981.

[33] C. Bohren and D. Huffman, *Absorption and Scattering of Light by Small Particles*, John Wiley & Sons, New York, NY, USA, 1983.

[34] A. Ishimaru, *Wave Propagation and Scattering in Random Media*, IEEE Press, Piscataway, NJ, USA, 1997.

[35] ASAP Technical Guide. Breault Research Organization, 2006.

[36] Th. Delonge and H. Fouckhardt, "Integrated optical detection cell based on Bragg reflecting waveguides," *Journal of Chromatography A*, vol. 716, no. 1-2, pp. 135–139, 1995.

[37] M. Grewe, A. Grosse, and H. Fouckhardt, "Theoretical and experimental investigations of the optical waveguiding properties of on-chip microfabricated capillaries," *Applied Physics B*, vol. 70, no. 6, pp. 839–847, 2000.

[38] A. Grosse, M. Grewe, and H. Fouckhardt, "Deep wet etching of fused silica glass for hollow capillary optical leaky waveguides in microfluidic devices," *Journal of Micromechanics and Microengineering*, vol. 11, no. 3, pp. 257–262, 2001.

[39] I. Steingoetter and H. Fouckhardt, "Deep fused silica wet etching using an Au-free and stress-reduced sputter-deposited Cr hard mask," *Journal of Micromechanics and Microengineering*, vol. 15, no. 11, pp. 2130–2135, 2005.

[40] http://www.schott.com/special_applications/english/proucts/thin_glass/thinglass.html.

[41] S. Burger, R. Koehle, L. Zschiedrich, et al., "Rigorous simulation of 3D masks," in *Photomask Technology*, vol. 6349 of *Proceedings of SPIE*, pp. 1–8, Monterey, Calif, USA, September 2006.

[42] J. Pomplun, S. Burger, F. Schmidt, et al., "Rigorous FEM-simulation of EUV-masks: influence of shape and material parameters," in *Photomask Technology*, vol. 6349 of *Proceedings of SPIE*, pp. 1–8, Monterey, Calif, USA, September 2006.

[43] S. Burger, R. Koehle, L. Zschiedrich, et al., "Benchmark of FEM, waveguide and FDTD algorithms for rigorous mask simulation," in *25th Annual BACUS Symposium on Photomask Technology*, vol. 5992 of *Proceedings of SPIE*, pp. 1–12, Monterey, Calif, USA, October 2005.

[44] L. Zschiedrich, S. Burger, R. Klose, A. Schaedle, and F. Schmidt, "JCMmode: an adaptive finite element solver for the computation of leaky modes," in *Integrated Optics: Devices, Materials, and Technologies IX*, vol. 5728 of *Proceedings of SPIE*, pp. 192–202, San Jose, Calif, USA, January 2005.

[45] W. Li, R. A. Jones, S. C. Allen, J. C. Heikenfeld, and A. J. Steckl, "Maximizing Alq_3 OLED internal and external efficiencies: charge balanced device structure and color conversion outcoupling lenses," *Journal of Display Technology*, vol. 2, no. 2, pp. 143–151, 2006.